Am J Transl Res 2020;12(10):6853-6867
www.ajtr.org /ISSN:1943-8141/AJTR0112497

Original Article

Tumor protein p53-induced nuclear protein 2 modulates osteogenic differentiation of human adipose derived stem/stromal cells by activating Wnt/β-catenin signaling

Shi Dong[1,2,3], Jie Li[1,2,3], Xiaonan Zhang[1,2,3]

[1]College of Stomatology, Chongqing Medical University, Chongqing, China; [2]Chongqing Key Laboratory of Oral Diseases and Biomedical Sciences, Chongqing, China; [3]Chongqing Municipal Key Laboratory of Oral Biomedical Engineering of Higher Education, Chongqing, China

Received April 13, 2020; Accepted July 25, 2020; Epub October 15, 2020; Published October 30, 2020

Abstract: Human adipose derived stem/stromal cells (hASCs) are frequently used as seed cells in bone tissue engineering. These cells have good osteogenic properties in various *in vivo* and *in vitro* models. Tumor protein p53-induced nuclear protein 2 (TP53INP2) regulates apoptosis, autophagy, and cell differentiation. However, whether TP53INP2 regulates osteogenic differentiation of hASCs has not been sufficiently studied. Herein, we explored this topic using siRNA experiments, osteogenic induction, quantitative real-time PCR (qRT-PCR) and western blot analysis. We found that siRNA decreased mRNA levels of osteoblast-specific genes in TP53INP2 cells. Western blots showed that RUNX2 protein expression decreased in siRNA-TP53INP2 cells at day 3, 7, and 21 after osteogenic induction. The level of β-catenin, LC3 and the LC3-II/LC3-I ratio in siRNA-TP53INP2 cells was decreased at day 3 and 7 after osteogenic induction. Further, treatment with lithium chloride (LiCl), an activator of Wnt signaling pathway, induced partial recovery of protein expression of β-catenin and RUNX2 (osteoblast-specific factor 2) in TP53INP2 knockdown cells. Collectively, these results show that TP53INP2 promotes osteogenic differentiation of hASCs by activating Wnt/β-catenin signaling.

Keywords: TP53INP2, hASCs, osteogenic differentiation, Wnt/β-catenin, autophagy

Introduction

Trauma, tumors and congenital diseases have been found to cause bone tissue defects, and even secondary deformities [1-3]. Currently, substantial research has been directed at studying the effective methods to repair bone defects. Human adipose derived stem/stromal cells (hASCs) can differentiate into adipocytes, osteoblasts, chondrocytes and myoblasts [4]. These cells possess multiple advantages including rich source for harvesting, ease of harvest through a non-invasive procedure, high acquisition efficiency and a good proliferative capacity *in vitro* [5]. In addition, multiple studies have reported that hASCs possess good osteogenic properties *in vivo* and *in vitro* [6-8]. Thus, hASCs have good prospects in bone tissue regeneration. However, there is limited knowledge about how their differentiation is regulated at the molecular level, which is needed to inform their future applications in the clinic.

Human tumor protein p53-induced nuclear protein 2 (TP53INP2) was first identified to be located on the long arm of chromosome 20 [9]. The protein encoded by the TP53INP2 bears homology to the tumor protein p53-induced nuclear protein 1 (TP53INP1) [10]. TP53INP2 is also called DOR (diabetes and obesity regulated protein) because it is under expressed in the Zucker diabetic fatty rat [11]. Its association with obesity in this animal model led to the hypothesis that TP53INP2 regulates adiposity. More recently, TP53INP2 expression was found to be downregulated in diabetes-free sWAT of obese patients [12].

Recent research has reported that TP53INP2 negatively modulates adipogenic differentiation of preadipocytes by activating β-catenin signaling [12]. Some studies have demonstrated that osteogenic differentiation of mesenchymal stem cells (MSCs) and adipogenic differentiation are opposite [13-15]. Currently, the role of TP53INP2 in osteogenic differentiation has not been sufficiently studied. By mediating the effects of the thyroid hormone in osteoblasts, TP53INP2 may regulate osteoblast differentiation [16]. Evidence indicates that the Wnt signaling pathway is an important regulator of osteogenic and adipogenic differentiation of MSCs [13, 17]. However, whether TP53INP2 regulates osteogenic differentiation of ASCs via Wnt pathway has not been previously interrogated.

In addition to its function as a modulator of cell differentiation, TP53INP2 is also involved in autophagy [18]. Loss of TP53INP2 in Drosophila melanogaster larvae fat has been shown to significantly impair autophagy [19]. Similarly, using a mouse model, TP53INP2 knockout in skeletal muscles impaired autophagy, which was rescued by its overexpression in the same tissue [20]. Together, these findings suggest that TP53INP2 is a positive modulator of autophagy. However, the role TP53INP2 in autophagy during osteogenic differentiation of hASCs is unclear.

In this study, the effects of TP53INP2 knockdown on osteogenic differentiation of hASCs were investigated by monitoring the expression of runt-related transcription factor 2 (RUNX2). The role of autophagy and the Wnt signaling pathway in this process were also investigated.

Materials and methods

Subjects

Human adipose tissues were obtained from five healthy women donors (18-35 years of age) scheduled to undergo liposuction for aesthetic purposes in the Plastic and Cosmetic Center in Hospital of Stomatology, Chongqing Medical University. None of the women had systemic diseases or infections. Informed consent was obtained from each woman. All experiments in this study were conducted in accordance with the Declaration of Helsinki following protocols reviewed and approved by Ethics Committee of College of Stomatology, Chongqing Medical University.

Cells isolation and culture

Fresh adipose tissues and excess tissues after liposuction were immediately transported to a laboratory. The tissues were washed with phosphate-buffered saline (PBS) (Solarbio, Beijing, China) to remove blood and grease, and then digested with 0.1% type I collagenase (Sigma-Aldrich, St. Louis, MO, USA) for one hour as previously described [21]. After digestion, tissues were shaken and centrifuged at 300 × *g* twice. After the last centrifugation, the upper layer of collagenase solution containing oil and fat was removed, and the cells in the bottom layer were harvested. Cells were resuspended in a given volume of PBS solution, washed, and centrifuged for 5 minutes at 300 × *g* repeatedly. Next, the upper PBS solution was discarded, and cells at the bottom of the tubes were cultured in a complete medium consisting of α-MEM (Hyclone, Logan, UT, USA), 10% fetal bovine serum (FBS, Gemini Bio-Products, Woodland, CA, USA) and 1% penicillin/streptomycin (HyClone, Logan, UT, USA) in an incubator. The medium was refreshed every 2 days. For LiCl treatment, cells were cultured in osteogenic inducing medium containing 5 mM LiCl (Sangon Biotech, Shanghai, China) for 7 days.

Flow cytometry analysis

The third generation of hASCs grown in 10 cm cell culture dish were trypsinized when they reached confluence, and 4 × 10^6 cells were resuspended in PBS containing 2% FBS in nine light-proof tube. After washing the cells three times with 2% FBS, cells were incubated with specific conjugated primary antibody and corresponding control for 30 minutes. Thereafter, cells were washed three times with 2% FBS, and analyzed with a BD Influx flow cytometer (BD Biosciences, San Jose, CA). The following human antibodies bought from BD Pharmingen™ (San Diego, CA, USA) were used: CD19-fluorescein isothiocyanate (FITC) (BD Biosciences, San Jose, CA, #560994), CD34-FITC (BD Biosciences, San Jose, CA, #555822), CD45-FITC (BD Biosciences, San Jose, CA, #560976), CD73-phycoerythrin (PE) (BD Biosciences, San Jose, CA, #550257), CD90-FITC (BD Biosciences, San Jose, CA, #555595),

CD105-FITC (BD Biosciences, San Jose, CA, #61443), CD146-PE (BD Biosciences, San Jose, CA, #550315), and STRO-1-FITC (BioLegend, San Diego, CA, USA, #340105).

Multilineage differentiation

hASCs were initially cultured in complete culture media until they reached 80% confluence. The medium was replaced with a fresh osteogenic induction medium (α-MEM supplemented with 10% FBS, 1% penicillin-streptomycin, 10 mM β-glycerophosphate (Sigma Aldrich, St. Louis, MO, USA), 50 mg/ml ascorbate (Sigma Aldrich, St. Louis, MO, USA), and 10 nM dexamethasone (DEX, Sigma Aldrich, St. Louis, MO, USA)); or adipogenic induction medium (α-MEM supplemented with 10% FBS, 1 mM DEX, 10 mM insulin, 200 mM indomethacin (Sigma Aldrich, St. Louis, MO, USA), and 0.5 mM 3-isobutyl-1-methylxantine (Sigma Aldrich, St. Louis, MO, USA)); or chondrogenic induction medium (Cyagen Biosciences Inc., Suzhou, China). The medium was refreshed every 2 days. Alizarin Red staining and Oil Red O staining were carried out after osteogenic induction for 21 days and adipogenic induction for 8 days, respectively. The staining of calcified nodules was eluted using 10% CPC in 10 mM sodium phosphate. The concentration of calcium was determined by measuring the absorbance at 540 nm with a multimode plate reader (PerkinElmer, USA). After chondrogenic induction for 30 days, the samples were prepared into paraffinized sections, and stained with Alcian Blue 8GX (Sigma-Aldrich, St. Louis, MO, USA).

Small interfering RNA (siRNA) knockdown

Three different siRNA sequences (siRNA-TP53IN-P2-homo-1901, siRNA-TP53INP2-homo-2668, siRNA-TP53INP2-homo-3762) and scrambled siRNA were designed and synthesized by Sangon Biotech (Shanghai, China). The sequences are as follows: TP53INP2-homo-1901-s: CCUGAAAUCUGAAGGGCUUTT, TP53-INP2-homo-1901-a: AAGCCCUUCAGAUUUCAGGTT, TP53INP2-homo-2668-s: GCAUUCCCAUGAGGGCAAATT, TP53INP2-homo-2668-a: UUUGCCCUCAUGGGAAUGCTT, TP53INP2-homo-3762-s: GCAACUUGCUCUGACCUAUTT, TP53-INP2-homo-3762-a: AUAGGUCAGAGCAAGUUGCTT, scrambled siRNA-s: UUCUCC GAACGUGUCACGUTT, scrambled siRNA-a: ACGUGACACGUUCGGAGAATT. The scrambled siRNA was used as a negative control (NC). When cells grew to 70% confluence in the 6-well plates, they were transfected with siRNA-TP53INP2 or scrambled siRNA, using Lipofectamine 3000 (Thermo Fisher Scientific, Waltham, MA, USA) transfection reagents following the manufacturer's protocol. After 48 h, the media were replaced with complete culture media. Lastly, knockdown of TP53INP2 was verified by quantitative real-time PCR, western blot and immunofluorescence staining.

RNA isolation, cDNA synthesis, quantitative real-time PCR (qRT-PCR)

RNAiso Plus reagent (Takara Biomedical Technology, Beijing, China) was used to extract total RNA from cells according to the manufacturer's instructions. cDNA was synthesized using a PrimeScript™ RT Master Mix (Perfect Real Time) (Takara Biomedical Technology, Beijing, China). According to the manufacturer's instructions, qRT-PCR was performed by using the QuantiNova SYBR Green PCR Kit (QIAGEN, Hilden, Germany). The primer sequences were as follows: GAPDH Fwd: CCCCACTTGATTTTGGAGGGA, Rev: AGGGCTGCTTTTAACTCTGGT, TP53INP2 Fwd: CCTCCCCTTCTCCTCCAGTAAA, Rev: AGCCCAAAATTCAGTCTCACCA, ALP Fwd: GGCCTGTACCATACAAGCCC, Rev: CCACGTAGACGAGGTAGTTGTG, RUNX2 Fwd: TGGTTACTGTCATGGCGGGTA, Rev: TCTCAGATCGTTGAACCTTGCTA, OCN Fwd: CACTCCTCGCCCTATTGGC, Rev: CCCTCCTGCTTGGACACAAAG, COL1A1 Fwd: GAGGGCCAAGACGAAGACATC, Rev: CAGATCACGTCATCGCACAAC.

Western blot

After washing three times with PBS, cells were treated with RIPA Lysis buffer containing Phenylmethanesulfonyl fluoride (PMSF) (Beyotime, Shanghai, China) to obtain total cellular protein. In order to quantify the concentration of protein, the Enhanced BCA Protein Assay Kit (Beyotime, Shanghai, China) was used. Next, protein sample was heated for 5 minutes with loading buffer (Beyotime, Shanghai, China). Then, 20 uL protein volume was separated on SDS-PAGE (Beyotime, Shanghai, China), and they were transferred onto PVDF membranes. Next, membranes were blocked in milk with 5% fat-free milk (Beyotime, Shanghai, China) for 2 hours. And they were incubated with anti-GAPDH (7E4) Mouse mAb (Zenbio, Chengdu, China,

#200306-7E4), anti-TP53INP2 Rabbit pAb (Zenbio, Chengdu, China, #251729), anti-RUNX2 (D1L7F) Rabbit mAb (CST, USA, #12556), anti-LC3A/B Rabbit pAb (Zenbio, Chengdu, China, #306019), anti-GSK3 beta (2E6) Mouse mAb (Zenbio, Chengdu, China, #200494-2E6), anti-Phospho-GSK3 beta (Ser9) Rabbit pAb (Zenbio, Chengdu, China, #310010), anti-beta Catenin (5D6) Mouse mAb (Zenbio, Chengdu, China, #201328-5D6), anti-SQSTM1/p62 Rabbit pAb (Zenbio, Chengdu, China, #380612), anti-Beclin-1 Rabbit pAb (Zenbio, Chengdu, China, #350130) at 4°C overnight. This was followed by incubation of membranes with the corresponding Goat anti-Rabbit IgG (H&L) (HRP conjugate) (Zenbio, Chengdu, China, #5112-03) or Goat anti-Mouse IgG (H&L) (HRP conjugate) (Zenbio, Chengdu, China, #511103) for 2 hours, respectively. Finally, the immunoblots were detected by chemiluminescence (Beyotime, Shanghai, China).

Statistical analysis

Using GraphPad Prism 6.0 software to analyze the data from the experimental results. One-way analysis of variance (ANOVA) was applied to compare means of multiple groups, and Dunnett's multiple comparison tests was used to post host test. Two-way ANOVA was used to analyze the experimental data of two factors, which was followed by Sidak's multiple comparison tests. Quantitative analyses of proteins levels were performed using Image J software. Data are shown as mean ± standard deviation (SD). Values of ****, $P < 0.0001$, ***, $P < 0.001$, **, $P < 0.01$, *, $P < 0.05$ showed statistical significance.

Results

Identification and characterization of hASCs

At the initial stage, the cells were small, polygonal, or spindle-shaped, with different sizes (**Figure 1A**). After culture for 8-9 days, the primary cells grew faster after passaging, acquiring a long spindle shape and uniform size (**Figure 1A**). The cells were then identified by flow cytometry. They tested positive for the following MSCs markers, CD73 (95.26%), CD90 (94.46%), CD105 (54.75%), and CD146 (43.35%). However, they poorly expressed CD19 (0.14%), CD34 (0.14%), CD45 (0.17%), and STRO-1 (0.30%) (**Figure 1B**).

Multilineage differentiation was performed for cells at third passage. Next, Alizarin Red S staining was done after culturing the cells in osteogenic induction medium for 21 days, Alizarin red positive calcium nodules were observed in the cells (**Figure 1C**). Lipid droplets were detected by Oil Red O staining after adipogenic induction (**Figure 1C**). Following 30 days of chondrogenic culture, the present of sulfated proteoglycans was analyzed by staining paraffin embedded sections with Alcian Blue (**Figure 1C**). In summary, these results reflect that hASCs can undergo multiple lineages of differentiation.

Transfection of small interfering RNA (siRNA)

Total RNA was extracted after 24 hours transfection and proteins was extracted after 48 hours transfection. Results showed that TP53INP2 expression levels were lower upon transfection with TP53INP2 siRNA compared to NC cells (**Figure 2A-D**).

Knockdown TP53INP2 inhibits osteogenic differentiation of hASCs

To determine whether TP53INP2 is required for osteogenic differentiation of hASCs, we carried out osteogenic induction for 21 days on TP53INP2 knockdown cells, NC cells and control cells. TP53INP2 knockdown cells exhibited less Alizarin Red S staining when compared to the NC cells (**Figure 3A**, **3B**). The same outcome was demonstrated by analysis of mineralized nodules following staining with 10% CPC (cetylpyridinium chloride) (**Figure 3C**). Next, we carried out osteogenic induction on the cells for 3 and 7 days. The expression levels of the osteoblast-specific genes alkaline phosphatase (ALP), type I collagen α1 (COL1A1) and osteocalcin (OCN) was determined. On day 3 of osteogenic induction, there was no significant change in expression of the aforementioned genes. RUNX2, a specific osteoblast marker was markedly reduced upon TP53INP2 knockdown (**Figure 3D**). On 7 days of osteogenic induction, mRNA levels of RUNX2, ALP, COL1A1, and OCN were significantly decreased in TP53INP2 knockdown cells (**Figure 3E**). Similar results were obtained at protein levels (**Figure 3F-K**).

Knockdown TP53INP2 decreases β-catenin level of hASCs

To explore the relationship between TP53INP2 and Wnt/β-catenin, we determined the protein

A

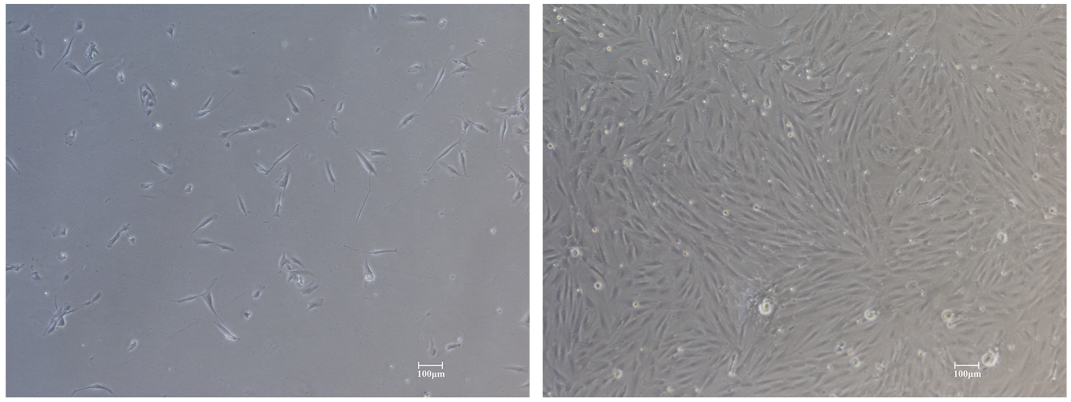
100μm
100μm

B

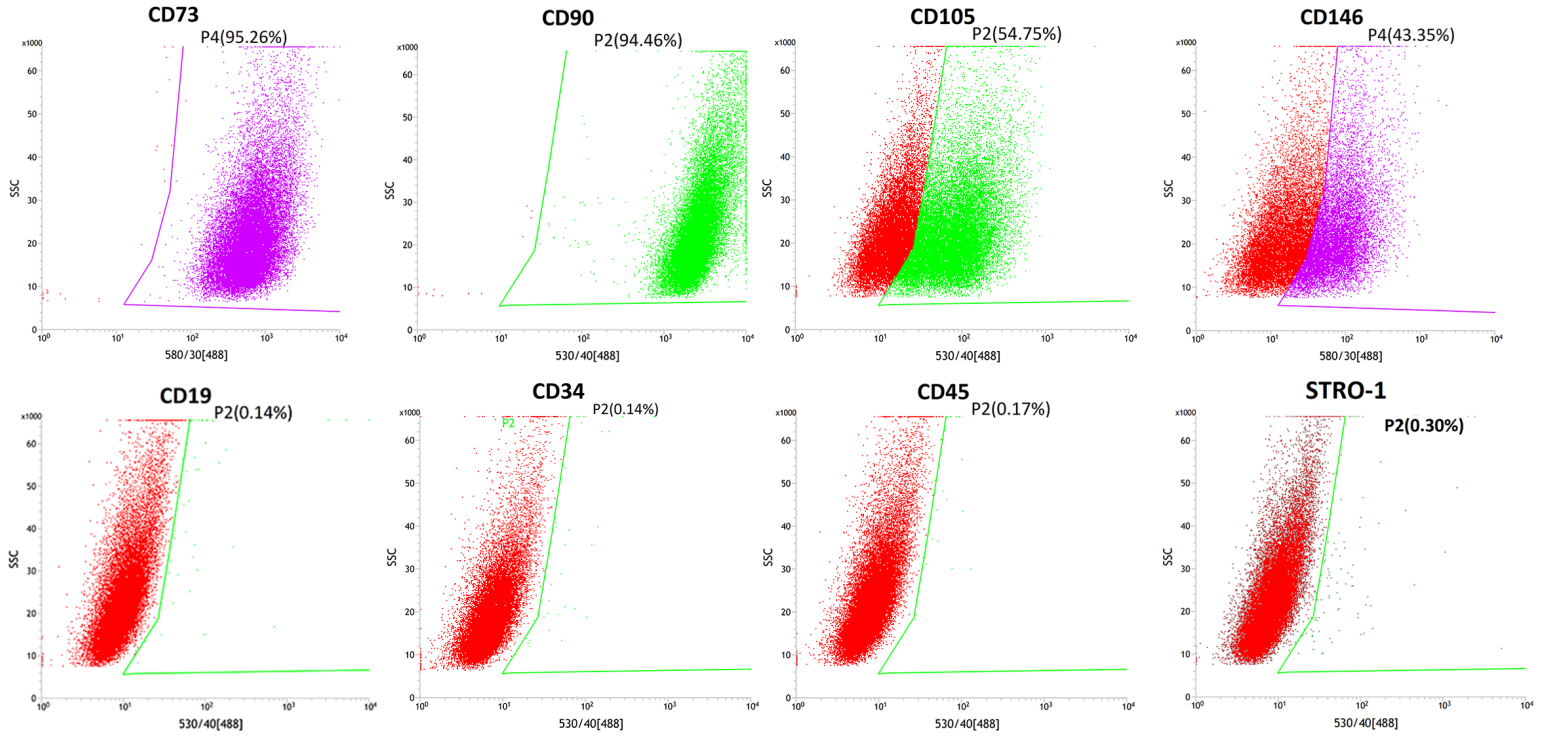
CD73
P4(95.26%)
CD90
P2(94.46%)
CD105
P2(54.75%)
CD146
P4(43.35%)
CD19
P2(0.14%)
CD34
P2(0.14%)
CD45
P2(0.17%)
STRO-1
P2(0.30%)
SSC
x1000
580/30[488]
530/40[488]

C

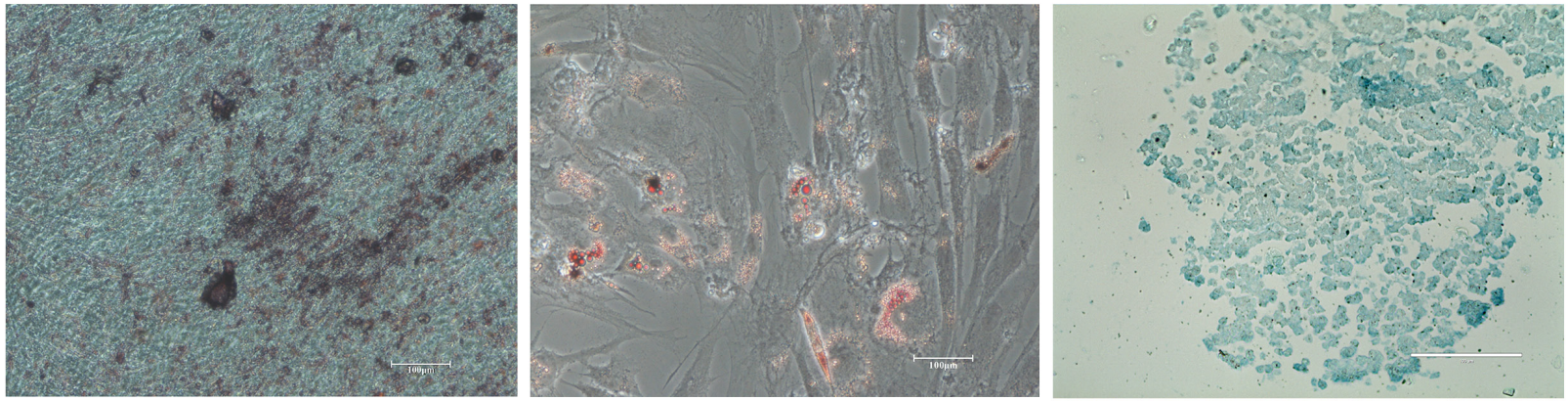

Figure 1. Identification and characterization of hASCs. A. The primary and the third passage hASCs were observed by light microscopy (scale bar 100 μm). B. hASCs Immunophenotypes analysis by flow cytometry: CD73(+) (95.26%), CD90(+) (94.46%), CD105(+) (54.75%), CD146(+) (43.35%), CD19(-) (0.14%), CD34(-) (0.14%), CD45(-) (0.17%), and STRO-1(-) (0.30%). C. Multilineage differentiation of hASCs. Mineralized nodules were detected by Alizarin Red S staining (on the left) (scale bar 100 μm); lipid droplets were detected by Oil Red O staining after 8 days of adipogenic induction (in the middle) (scale bar 100 μm); proteoglycan secretion were detected by Alcian Blue 8GX staining of paraffin section after 30 days of chondrogenic induction (on the right) (scale bar 100 μm).

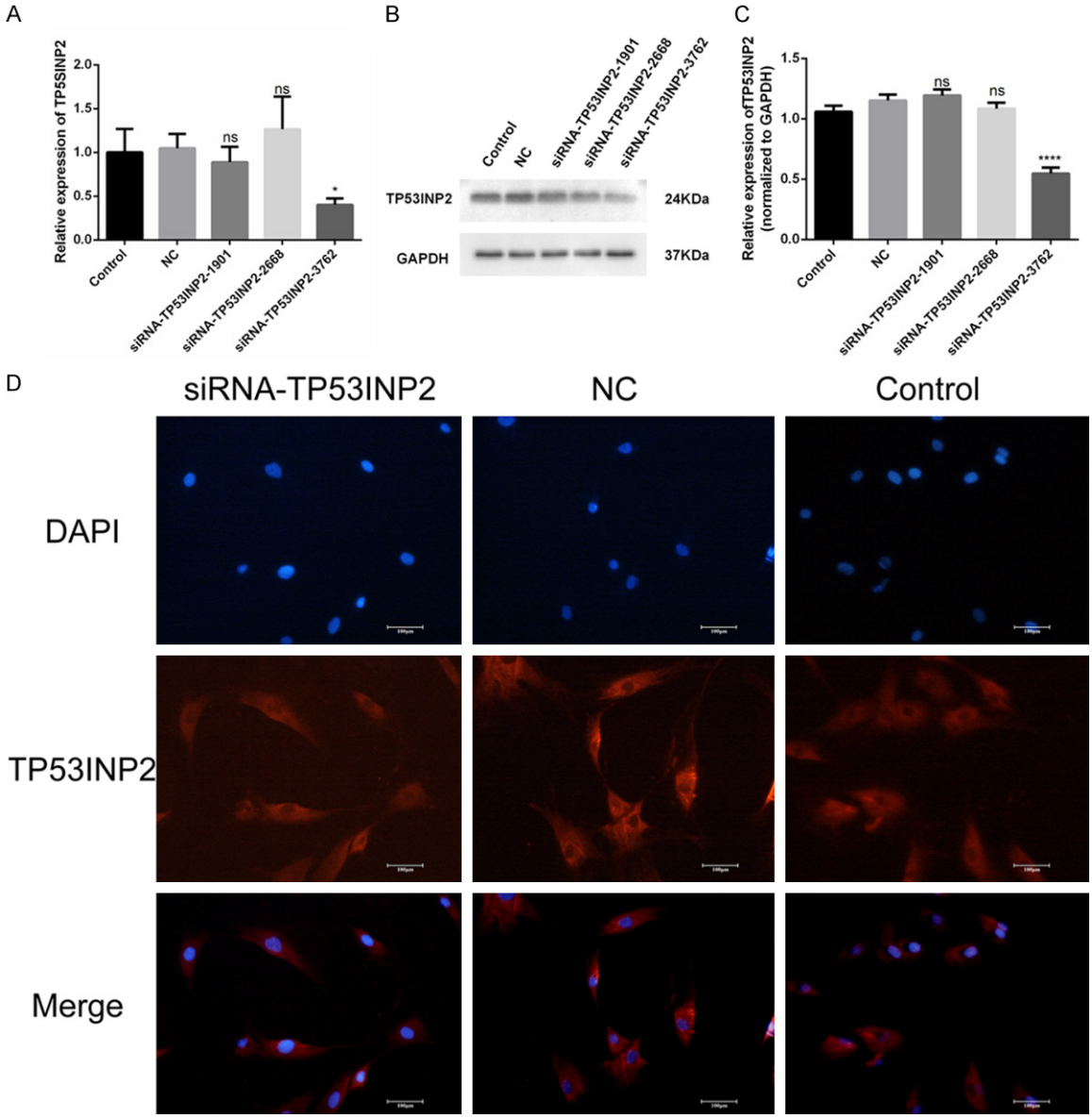

Figure 2. Transfection of small interfering RNA (siRNA). A. After transfection, appropriate siRNA-TP53INP2 sequence was screened by qRT-PCR, from three different sequences, including siRNA-TP53INP2-1901, siRNA-TP53INP2-2668 and siRNA-TP53INP2-3762. Data represent mean values ± SD (n = 3), *P < 0.05, One-way ANOVA and Dunnett's multiple comparison tests. B. Appropriate siRNA-TP53INP2 sequence was screened by western blot after transfection, and GAPDH was used as an internal standard. Data represent mean values ± SD (n = 3), ****P < 0.0001, One-way ANOVA and Dunnett's multiple comparison tests. C. Quantitative analyses of TP53INP2 protein level using Image J software. D. Immunofluorescence analysis of TP53INP2 expression after siRNA transfection 48 h. TP53INP2 was stained as red and nucleus were stained by DAPI showing blue. Bar: 100 μm.

levels of β-catenin in cells after 3 and 7 days of osteogenic induction. Results revealed a significant reduction in β-catenin protein levels upon TP53INP2 knockdown after both 3 and 7 days of osteogenic induction (**Figure 4A**, **4B**, **4D**). However, the protein levels of glycogen synthase kinase 3β (GSK-3β) were not altered after TP53INP2 knockdown (**Figure 4A**, **4C**, **4E**). Together, these results suggest that TP53INP2 might positively regulate β-catenin expression.

TP53INP2 regulates osteogenic differentiation of hASCs through the Wnt/β-catenin pathway

To further determine whether the role of TP53INP2 in osteogenic differentiation of hASCs was mediated by Wnt/β-catenin signaling, lithi-

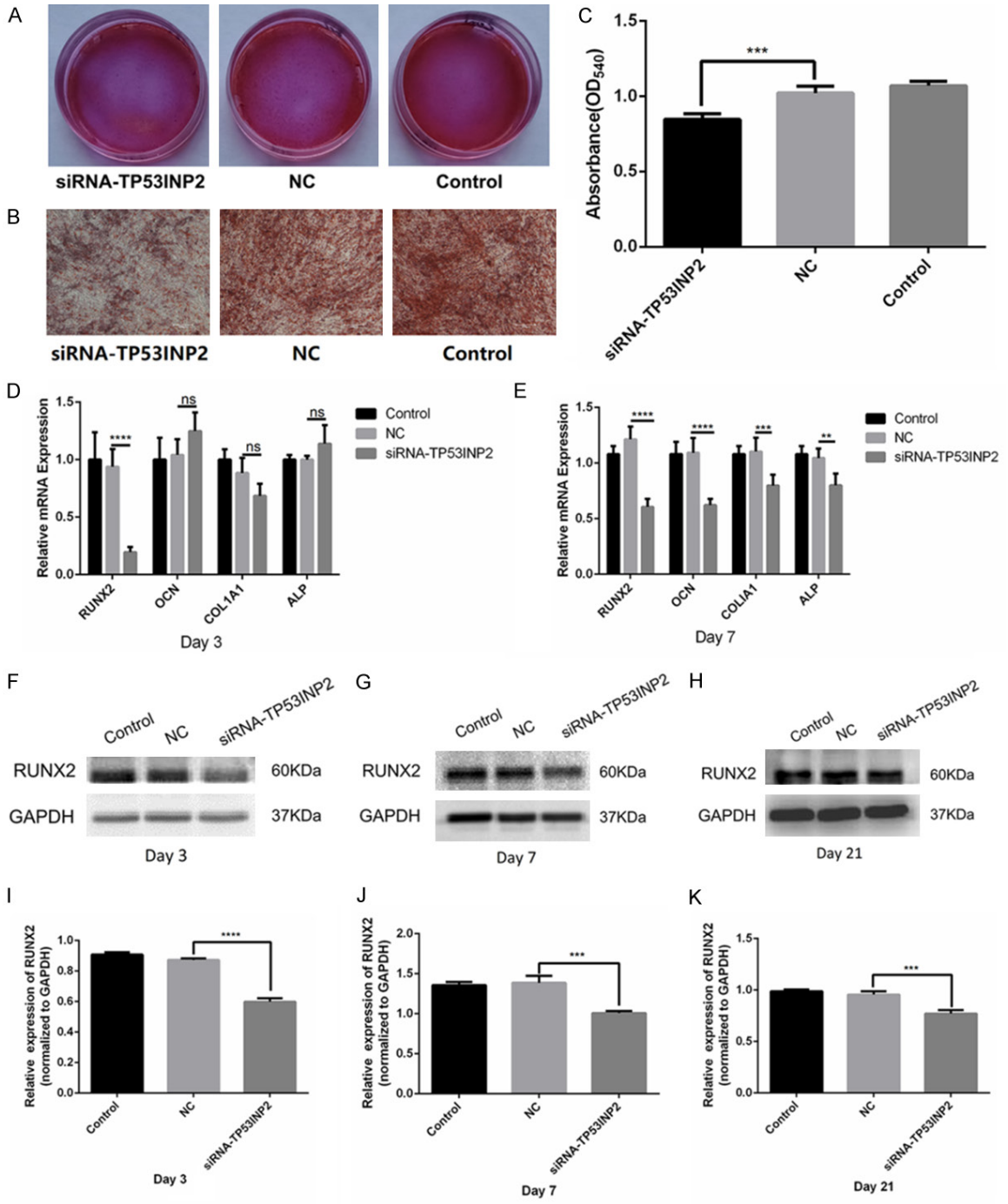

Figure 3. Knockdown TP53INP2 inhibits osteogenic differentiation of hASCs. A. Mineralized nodule formation was detected by Alizarin Red S staining on day 21 osteogenic differentiation. The siRNA-TP53INP2 cells had less intensive staining than that of in NC cells. B. The typical microscopic views of the three groups of cells (siRNA-TP53INP2, NC and control cells) were shown. C. Quantitative analysis of the staining of mineralized nodules were also shown. Data were expressed as the mean ± SD (n = 3, ***P < 0.001), One-way ANOVA and Dunnett's multiple comparison tests. D, E. The mRNA levels of RUNX2, OCN, COL1A1 and ALP were detected by qRT-PCR on day 3 and day 7 osteogenic induction. Data represent mean values ± SD (n = 3), **P < 0.01, ***P < 0.001, ****P < 0.0001, One-way ANOVA and Dunnett's multiple comparison tests. F-H. Western blots showed RUNX2 expression in siRNA-TP53INP2, NC and control cells on day 3, 7, 21 osteogenic induction, and GAPDH was used as an internal standard. I-K. Quantitative analyses of RUNX2 protein level using Image J software (mean values ± SD, n = 3), ***P < 0.001, ****P < 0.0001, One-way ANOVA and Dunnett's multiple comparison tests.

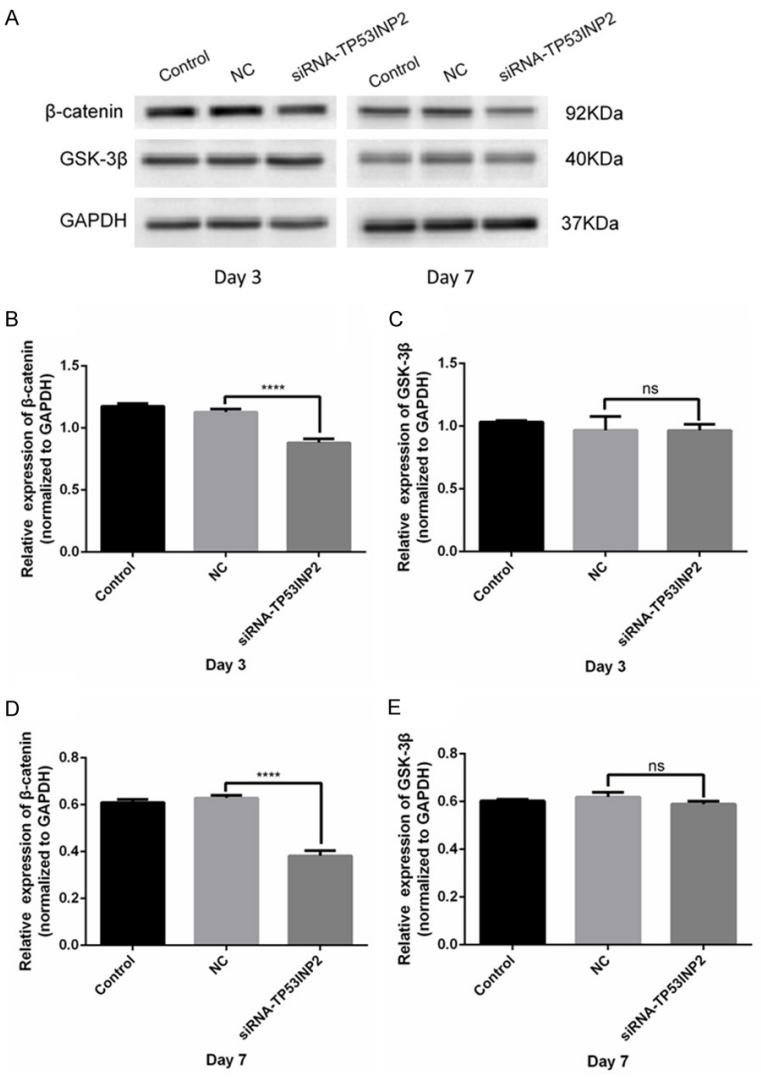

Figure 4. Knockdown TP53INP2 decreases β-catenin level in hASCs. A. Western blot analysis of β-catenin and GSK-3β expressions in hASCs (siRNA-TP53INP2, NC and control) on day 3 and 7 osteogenic induction, and GAPDH was used as internal standard. B, C. Quantitative analyses of β-catenin and GSK-3β protein levels of hASCs on day 3 osteogenic induction using Image J software (mean values ± SD, n = 3), ****P < 0.0001, One-way ANOVA and Dunnett's multiple comparison tests. D, E. Quantitative analyses of β-catenin and GSK-3β protein levels of hASCs on day 7 osteogenic induction using Image J software (mean values ± SD, n = 3), ****P < 0.0001, One-way ANOVA and Dunnett's multiple comparison tests.

um chloride (LiCl) was used to activate this pathway. During osteogenic differentiation of hASCs, and monitored the pathway's activation status by montitoring the level phosphorylated GSK-3β (p-GSK-3β), which is regarded as the inactive state of GSK-3β [22]. Results indicated that the protein level of p-GSK-3β and β-catenin following treatment of the cells with LiCl were elevated, indicating activation of Wnt signaling (**Figure 5A**, **5B**, **5D**). Interestingly, the increase in p-GSK-3β induced by LiCl was more pronounced in cells with TP53INP2 knockdown relative to the NC cells (**Figure 5A**, **5D**). Additionally, TP53-INP2 silencing reduced expression of β-catenin, which was rescued by LiCl treatment (**Figure 5A**, **5B**). Notably, RUNX2 expression upon TP53-INP2 knockdown rose significantly following LiCl treatment (**Figure 5A**, **5F**). Interestingly, western blot analysis revealed increased TP53INP2 expression in TP53INP2 knockdown cells after activating Wnt signaling pathway (**Figure 5A**, **5E**).

Inhibition of TP53INP2 influenced autophagy in hASCs during osteogenic differentiation

Although the role of TP53INP2 in autophagy has been well documented, it is not clear whether silencing affects autophagy during osteogenic induction. Here, we found that the expression levels of the autophagy markers LC3, LC3-II/LC3-I ratio and P62 were decreased following TP53INP2 knockdown cells after 3 and 7 days of osteogenic induction (**Figure 6A-C**, **6E-G**, **6I**). However, there was no appreciable change in Beclin1 levels after TP53INP2 knockdown after 3 days of induction. By contrast, Beclin1 protein levels were clearly reduced after TP53INP2 knockdown following 7 days of induction (**Figure 6A**, **6D**, **6H**).

Discussion

ASCs are commonly used in bone tissue engineering owing to their good osteogenic differentiation capacity [23-25]. So far, several studies have revealed that the Wnt pathway [26-28], BMP signaling [29, 30], Notch signaling [31],

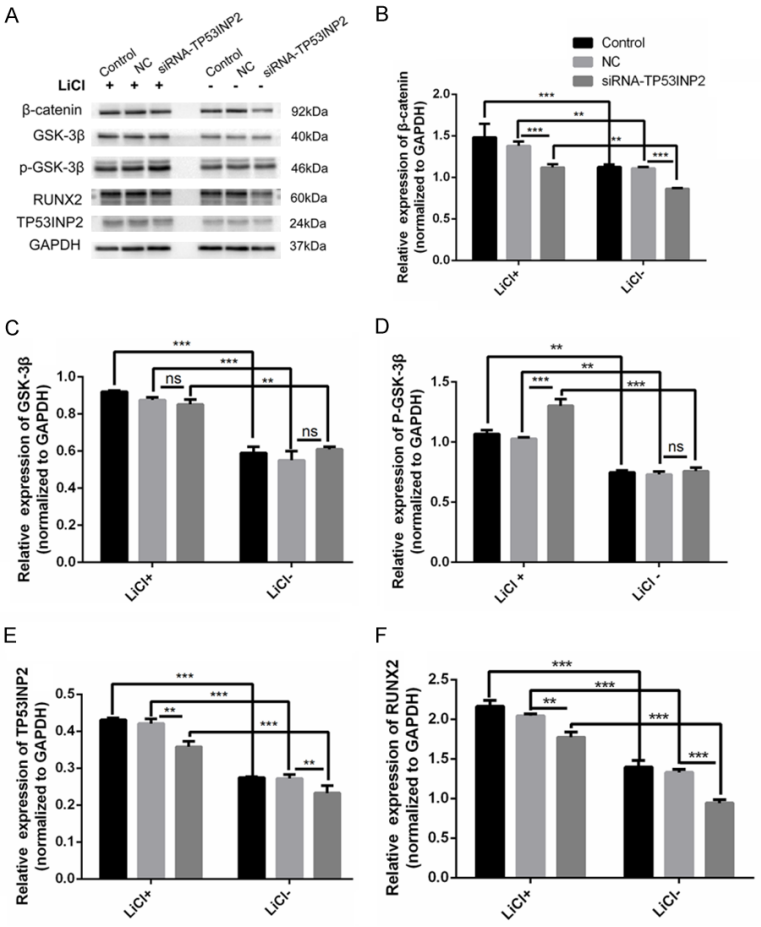

Figure 5. TP53INP2 regulates osteogenic differentiation of hASCs through Wnt/β-catenin pathway. A. Representative Western blots showed that the levels of β-catenin, GSK-3β, p-GSK-3β, RUNX2, and TP53INP2 in hASCs (siRNA-TP53INP2, NC and control) after 7 days treatment of osteogenic medium with LiCl. GAPDH was used as internal standard. B-F. Quantitative analyses of β-catenin, GSK-3β, p-GSK-3β, TP53INP2, and RUNX2 in hASCs (siRNA-TP53INP2, NC and control) after 7 days treatment of osteogenic medium with LiCL, using Image J software, respectively. Data represent mean values ± SD (n = 3), **P < 0.01, ***P < 0.001, Two-way ANOVA and Sidak's multiple comparisons tests.

VEGF signaling participate in the molecular mechanisms of osteogenic differentiation of ASCs [32, 33]. RUNX2 is well-known as a master regulator of the transcription of genes during osteoblast differentiation [34, 35]. TP53INP2 has a negative role in adiposity regulation, and positively modulates autophagy [12, 18, 19]. However, the impact of TP53INP2 expression on osteogenic differentiation in hASCs has so far not been investigated. Its role in diabetes, fat metabolism, apoptosis, and tumor or genesis has however been reported [12, 20, 36-38]. It has been previously reported that TP53INP2 modulates thyroid hormone mediated osteoblast differentiation [16]. We also reported that TP53INP2 silencing inhibited the expression of RUNX2, ALP, OCN and COL1A1, and suppressed the formation of mineralized nodules. Western blot analysis revealed a significant reduction in RUNX2 protein levels upon TP53INP2 knockdown during osteogenic induction (**Figure 3**). These results demonstrated that TP53INP2 functions a positive regulator during osteogenic differentiation of hASCs. Coupled with the previously reported negative effect of TP53INP2 on adipogenic differentiation [12], our findings confirmed the existence of an opposite relationship between osteogenic differentiation and adipogenic differentiation of MSCs [13, 39].

As we known, β-catenin plays the central role in the mediation of canonical Wnt signaling [40, 41]. After activating the cannonical Wnt signaling pathway, β-catenin translocates into the nucleus [42]. Western blot analysis showed that silencing TP53INP2 significantly reduced β-catenin levels during osteogenic induction (**Figure 4A**, **4B**, **4D**). Similar findings have been reported previously in TP53INP2-deficient 3T3-L1 preadipocytes [12]. This implies that TP53INP2 modulates β-catenin expression level in hASCs during osteogenic differentiation.

To further investigate the role of Wnt signaling in this process, LiCl, a GSK3 inhibitor, was used to activate Wnt/β-catenin signaling pathway. Analysis of the results revealed that protein levels of β-catenin, GSK-3β and p-GSK-3β were elevated by LiCl (**Figure 5A-D**), indicating activation of Wnt/β-catenin signaling. Additionally, p-GSK-3β expression was markedly higher in TP53INP2 knockdown cells relative to the NC cells. Together, these findings indicate that

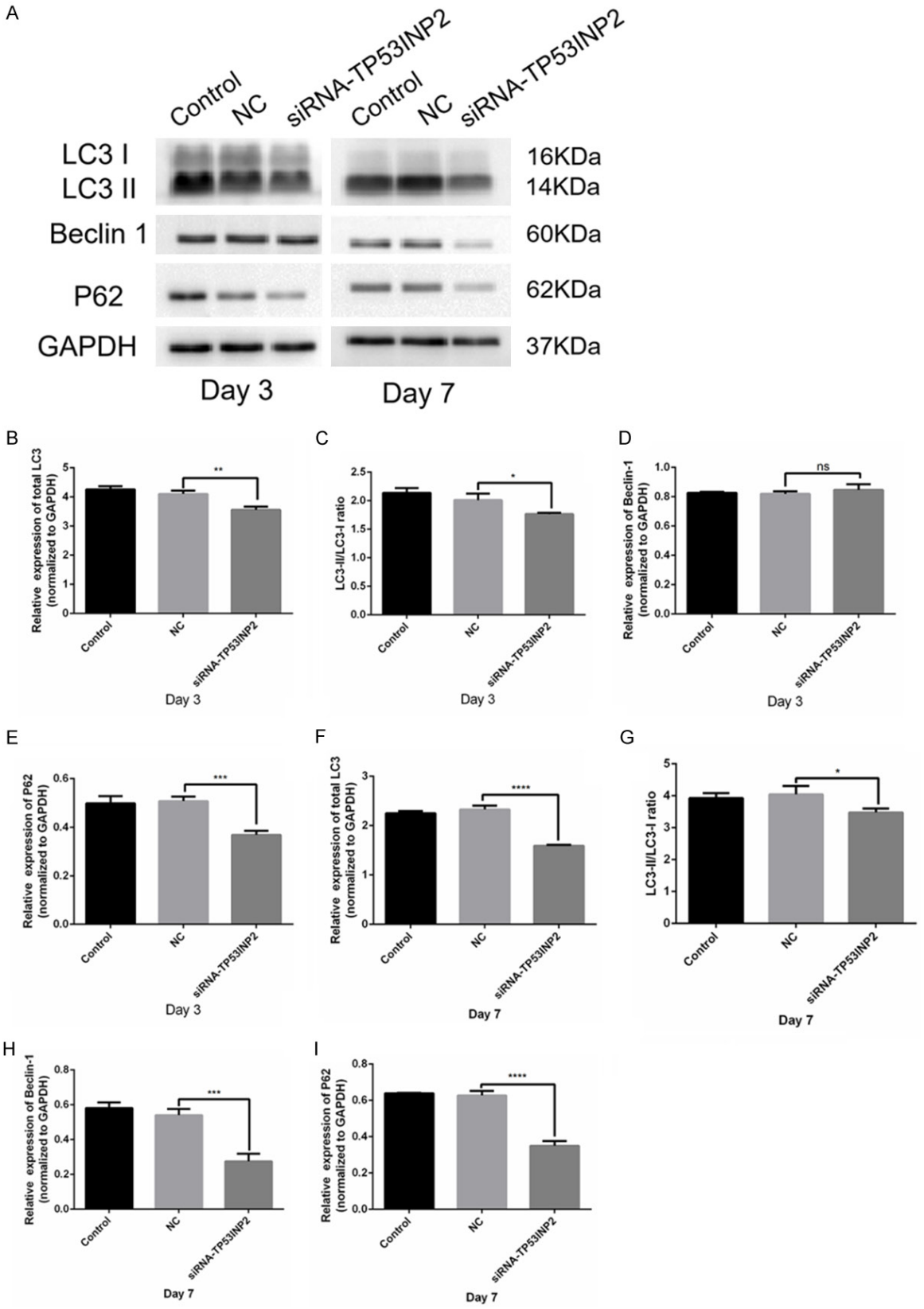

Figure 6. Inhibition of TP53INP2 influences autophagy in hASCs during osteogenic differentiation. A. Western blot analysis of LC3, Beclin1 and P62 expressions of hASCs (siRNA-TP53INP2, NC and control) on day 3 and 7 osteogenic induction, and GAPDH was used as internal standard. B-E. Quantitative analyses of LC3, LC3 II/LC3 I ratio, Beclin1

and P62 expression levels of hASCs (siRNA-TP53INP2, NC and control) on day 3 osteogenic induction, using Image J software, respectively. Data represent mean values ± SD (n = 3), *P < 0.05, **P < 0.01, ***P < 0.001, One-way ANOVA and Dunnett's multiple comparison tests. F-I. Quantitative analyses of LC3, LC3 II/LC3 I ratio, Beclin1 and P62 expression levels of hASCs (siRNA-TP53INP2, NC and control) on day 7 osteogenic induction, using Image J software, respectively. Data represent mean values ± SD (n = 3), *P < 0.05, ***P < 0.001, ****P < 0.0001, One-way ANOVA and Dunnett's multiple comparison tests.

TP53INP2 knockdown enhanced the phosphorylation of GSK-3β by LiCl. Notably, LiCl rescued β-catenin expression in TP53INP2 knockdown cells. These results support a previous report that TP53INP2-deficicent preadipocytes express low levels of β-catenin, which is rescued by Wnt3a-mediated activation of the Wnt signaling pathway [12]. Additionally, we observed that RUNX2 expression in TP53INP2 knockdown cells was partially rescued by LiCl driven activation of the Wnt pathway (**Figure 5A** and **5F**). It has been reported that Wnt3a mediates activation of β-catenin in TP53INP2-deficient 3T3-L1 cells while repression of the adipogenic markers PPAR-γ and C/EBP-α results suppression of adipogenesis [12]. Generally, our results illustrate that TP53INP2 activates Wnt/β-catenin signaling pathway, which in turn up-regulates RUNX2, a downstream target of Wnt. Surprisingly, LiCl treatment increased the protein level of TP53INP2 (**Figure 5A** and **5E**). This observation suggests that the Wnt/β-catenin pathway and TP53INP2 may form a positive feedback loop or Wnt/β-catenin pathway activates TP53INP2 expression.

Autophagy is a catabolic process in which proteins and damaged organelles are engulfed by autophagosomes lysosomal degradation [43]. This process maintains stemness and cell differentiation [44]. During autophagy, LC3-I, a cytoplasmic form of LC3, is gradually lipidized by Atg3, Atg7 and Atg16/Atg12-Atg5 complex to form LC3-II [45]. Our analysis revealed that TP53INP2 knockdown during osteogenic induction impaired autophagy as revealed by the decreased LC3-II to LC3-I ratio and reduction in the total LC3 level (**Figure 5**). This suggests that TP53INP2 is a positive modulator of autophagy [19, 20]. Previous reports have suggested that TP53INP2 modulates autophagy by interacting with LC3 or LC3-related proteins and transports them to the autophagosome through vacuole membrane protein 1 (VMP1) [10]. When autophagy is activated, TP53INP2 exits the nucleus and initiates the the formation of autophagic membranes in cooperation with LC3 in the cytoplasm, which mediates the formation of autophagosome by LC3-ATG7 [46]. We speculate that the knockdown of TP53INP2 might affect these processes, thereby inhibit osteogenic differentiation by suppressing autophagy. Moreover, we also shown that TP53INP2 knockdown reduced expression of P62 during osteogenic induction. Similar outcomes were obtained upon TP53INP2 overexpression in C2C12 myotubes [20]. This might result from a competition between TP53INP2 and P62 for LC3 [47, 48]. Some researches have reported that autophagy has a positive role in early osteogenesis of stem cells [49, 50]. Beclin1 dependent autophagy has been reported to drive osteogenic differentiation of human gingival mesenchymal stem cells [49]. Autophagy can promote osteogenic differentiation of human bone marrow mesenchymal stem cells [50]. Our results therefore suggest that autophagy might play a positive role TP53INP2 mediated osteogenic differentiation of hASCs.

In conclusion, this study demonstrates for the first time that TP53INP2 promotes osteogenic differentiation of hASCs by activating Wnt/β-catenin signaling. And autophagy is closely related to the regulation of TP53INP2 on osteogenic differentiation of hASCs, but further study is needed. The findings of this study lay a foundation for further research into the mechanism of TP53INP2 in the osteogenic differentiation of hASCs, and reveal an avenue for targeting TP53INP2 to repair bone defects.

Acknowledgements

This work was supported by the National Natural Science Foundation of China (Grant No. 81700982 and 81700932), Chongqing Research Program of Basic Research and Frontier Technology (Grant No. cstc2017jcyjAX0454) and Chongqing Municipal Studios for Young and Middle-aged Top Medical Talents (ZQNYXGDRCGZS2019004).

Disclosure of conflict of interest

None.

Address correspondence to: Dr. Jie Li, College of Stomatology, Chongqing Medical University, 426# Songshibei Road, Yubei District, Chongqing 401147, P. R. China. Tel: +86-23-8860-2351; Fax: +86-23-8886-0222; E-mail: jieli@hospital.cqmu.edu.cn; Dr. Xiaonan Zhang, College of Stomatology, Chongqing Medical University, 426# Songshibei Road, Yubei District, Chongqing 401147, P. R. China. Tel: +86-23-8903-5721; Fax: +86-23-8886-0222; E-mail: 500133@hospital.cqmu.edu.cn

References

[1] Makris EA, Gomoll AH, Malizos KN, Hu JC and Athanasiou KA. Repair and tissue engineering techniques for articular cartilage. Nat Rev Rheumatol 2015; 11: 21-34.

[2] Li G, Zhou T, Lin S, Shi S and Lin Y. Nanomaterials for craniofacial and dental tissue engineering. J Dent Res 2017; 96: 725-732.

[3] Jazayeri HE, Tahriri M, Razavi M, Khoshroo K, Fahimipour F, Dashtimoghadam E, Almeida L and Tayebi L. A current overview of materials and strategies for potential use in maxillofacial tissue regeneration. Mater Sci Eng C Mater Biol Appl 2017; 70: 913-929.

[4] Ciuffi S, Zonefrati R and Brandi ML. Adipose stem cells for bone tissue repair. Clin Cases Miner Bone Metab 2017; 14: 217-226.

[5] Zuk PA, Zhu M, Mizuno H, Huang J, Futrell JW, Katz AJ, Benhaim P, Lorenz HP and Hedrick MH. Multilineage cells from human adipose tissue: implications for cell-based therapies. Tissue Eng 2001; 7: 211-228.

[6] Dufrane D. Impact of age on human adipose stem cells for bone tissue engineering. Cell Transplant 2017; 26: 1496-1504.

[7] Wagner W, Wein F, Seckinger A, Frankhauser M, Wirkner U, Krause U, Blake J, Schwager C, Eckstein V, Ansorge W and Ho AD. Comparative characteristics of mesenchymal stem cells from human bone marrow, adipose tissue, and umbilical cord blood. Exp Hematol 2005; 33: 1402-1416.

[8] Zuk PA, Zhu M, Ashjian P, De Ugarte DA, Huang JI, Mizuno H, Alfonso ZC, Fraser JK, Benhaim P and Hedrick MH. Human adipose tissue is a source of multipotent stem cells. Mol Biol Cell 2002; 13: 4279-4295.

[9] Nowak J, Depetris D, Iovanna JL, Mattei MG and Pebusque MJ. Assignment of the tumor protein p53 induced nuclear protein 2 (TP53INP2) gene to human chromosome band 20q11.2 by in situ hybridization. Cytogenet Genome Res 2005; 108: 362.

[10] Nowak J, Archange C, Tardivel-Lacombe J, Pontarotti P, Pebusque MJ, Vaccaro MI, Velasco G, Dagorn JC and Iovanna JL. The TP53INP2 protein is required for autophagy in mammalian cells. Mol Biol Cell 2009; 20: 870-881.

[11] Baumgartner BG, Orpinell M, Duran J, Ribas V, Burghardt HE, Bach D, Villar AV, Paz JC, Gonzalez M, Camps M, Oriola J, Rivera F, Palacin M and Zorzano A. Identification of a novel modulator of thyroid hormone receptor-mediated action. PLoS One 2007; 2: e1183.

[12] Romero M, Sabate-Perez A, Francis VA, Castrillon-Rodriguez I, Diaz-Ramos A, Sanchez-Feutrie M, Duran X, Palacin M, Moreno-Navarrete JM, Gustafson B, Hammarstedt A, Fernandez-Real JM, Vendrell J, Smith U and Zorzano A. TP53INP2 regulates adiposity by activating beta-catenin through autophagy-dependent sequestration of GSK3beta. Nat Cell Biol 2018; 20: 443-454.

[13] James AW. Review of signaling pathways governing MSC osteogenic and adipogenic differentiation. Scientifica (Cairo) 2013; 2013: 684736.

[14] Yuan Z, Li Q, Luo S, Liu Z, Luo D, Zhang B, Zhang D, Rao P and Xiao J. PPARgamma and wnt signaling in adipogenic and osteogenic differentiation of mesenchymal stem cells. Curr Stem Cell Res Ther 2016; 11: 216-225.

[15] Li Y, Jin D, Xie W, Wen L, Chen W, Xu J, Ding J and Ren D. PPAR-gamma and wnt regulate the differentiation of MSCs into adipocytes and osteoblasts respectively. Curr Stem Cell Res Ther 2018; 13: 185-192.

[16] Linares GR, Xing W, Burghardt H, Baumgartner B, Chen ST, Ricart W, Fernandez-Real JM, Zorzano A and Mohan S. Role of diabetes- and obesity-related protein in the regulation of osteoblast differentiation. Am J Physiol Endocrinol Metab 2011; 301: E40-48.

[17] Zhou X, Liu Z, Huang B, Yan H, Yang C, Li Q and Jin D. Orcinol glucoside facilitates the shift of MSC fate to osteoblast and prevents adipogenesis via Wnt/beta-catenin signaling pathway. Drug Des Devel Ther 2019; 13: 2703-2713.

[18] Sancho A, Duran J, Garcia-Espana A, Mauvezin C, Alemu EA, Lamark T, Macias MJ, DeSalle R, Royo M, Sala D, Chicote JU, Palacin M, Johansen T and Zorzano A. DOR/Tp53inp2 and Tp53inp1 constitute a metazoan gene family encoding dual regulators of autophagy and transcription. PLoS One 2012; 7: e34034.

[19] Mauvezin C, Orpinell M, Francis VA, Mansilla F, Duran J, Ribas V, Palacin M, Boya P, Teleman AA and Zorzano A. The nuclear cofactor DOR regulates autophagy in mammalian and Drosophila cells. EMBO Rep 2010; 11: 37-44.

[20] Sala D, Ivanova S, Plana N, Ribas V, Duran J, Bach D, Turkseven S, Laville M, Vidal H, Karczewska-Kupczewska M, Kowalska I, Straczkowski M, Testar X, Palacin M, Sandri M, Serrano AL and Zorzano A. Autophagy-regulating

TP53INP2 mediates muscle wasting and is repressed in diabetes. J Clin Invest 2014; 124: 1914-1927.

[21] Li J, Curley JL, Floyd ZE, Wu X, Halvorsen YDC and Gimble JM. Isolation of human adipose-derived stem cells from lipoaspirates. Methods Mol Biol 2018; 1773: 155-165.

[22] Hu L, Su P, Yin C, Zhang Y, Li R, Yan K, Chen Z, Li D, Zhang G, Wang L, Miao Z, Qian A and Xian CJ. Microtubule actin crosslinking factor 1 promotes osteoblast differentiation by promoting beta-catenin/TCF1/Runx2 signaling axis. J Cell Physiol 2018; 233: 1574-1584.

[23] Linh NTB, Abueva CDG, Jang DW and Lee BT. Collagen and bone morphogenetic protein-2 functionalized hydroxyapatite scaffolds induce osteogenic differentiation in human adipose-derived stem cells. J Biomed Mater Res B Appl Biomater 2020; 108: 1363-1371.

[24] Wagner JM, Conze N, Lewik G, Wallner C, Brune JC, Dittfeld S, Jaurich H, Becerikli M, Dadras M, Harati K, Fischer S, Lehnhardt M and Behr B. Bone allografts combined with adipose-derived stem cells in an optimized cell/volume ratio showed enhanced osteogenesis and angiogenesis in a murine femur defect model. J Mol Med (Berl) 2019; 97: 1439-1450.

[25] Sattary M, Rafienia M, Kazemi M, Salehi H and Mahmoudzadeh M. Promoting effect of nano hydroxyapatite and vitamin D3 on the osteogenic differentiation of human adipose-derived stem cells in polycaprolactone/gelatin scaffold for bone tissue engineering. Mater Sci Eng C Mater Biol Appl 2019; 97: 141-155.

[26] Yuan C, Gou X, Deng J, Dong Z, Ye P and Hu Z. FAK and BMP-9 synergistically trigger osteogenic differentiation and bone formation of adipose derived stem cells through enhancing Wnt-beta-catenin signaling. Biomed Pharmacother 2018; 105: 753-757.

[27] Wang W, Wang S, Liu X, Gu R, Zhu Y, Zhang P, Liu Y and Zhou Y. Knockdown of ARL4C inhibits osteogenic differentiation of human adipose-derived stem cells through disruption of the Wnt signaling pathway. Biochem Biophys Res Commun 2018; 497: 256-263.

[28] Fathi E and Farahzadi R. Enhancement of osteogenic differentiation of rat adipose tissue-derived mesenchymal stem cells by zinc sulphate under electromagnetic field via the PKA, ERK1/2 and Wnt/beta-catenin signaling pathways. PLoS One 2017; 12: e0173877.

[29] Fan J, Park H, Tan S and Lee M. Enhanced osteogenesis of adipose derived stem cells with Noggin suppression and delivery of BMP-2. PLoS One 2013; 8: e72474.

[30] Vanhatupa S, Ojansivu M, Autio R, Juntunen M and Miettinen S. Bone morphogenetic protein-2 induces donor-dependent osteogenic and adipogenic differentiation in human adipose stem cells. Stem Cells Transl Med 2015; 4: 1391-1402.

[31] Fan C, Jia L, Zheng Y, Jin C, Liu Y, Liu H and Zhou Y. MiR-34a promotes osteogenic differentiation of human adipose-derived stem cells via the RBP2/NOTCH1/CYCLIN D1 coregulatory network. Stem Cell Reports 2016; 7: 236-248.

[32] Kedong S, Wenfang L, Yanxia Z, Hong W, Ze Y, Mayasari L and Tianqing L. Dynamic fabrication of tissue-engineered bone substitutes based on derived cancellous bone scaffold in a spinner flask bioreactor system. Appl Biochem Biotechnol 2014; 174: 1331-1343.

[33] Li Q, Wang T, Zhang GF, Yu X, Zhang J, Zhou G and Tang ZH. A comparative evaluation of the mechanical properties of two calcium phosphate/collagen composite materials and their osteogenic effects on adipose-derived stem cells. Stem Cells Int 2016; 2016: 6409546.

[34] Franceschi RT, Xiao G, Jiang D, Gopalakrishnan R, Yang S and Reith E. Multiple signaling pathways converge on the Cbfa1/Runx2 transcription factor to regulate osteoblast differentiation. Connect Tissue Res 2003; 44 Suppl 1: 109-116.

[35] Komori T. Regulation of osteoblast differentiation by Runx2. Adv Exp Med Biol 2010; 658: 43-49.

[36] Moran-Jones K, Grindlay J, Jones M, Smith R and Norman JC. hnRNP A2 regulates alternative mRNA splicing of TP53INP2 to control invasive cell migration. Cancer Res 2009; 69: 9219-9227.

[37] An J, Enomoto A, Weng L, Kato T, Iwakoshi A, Ushida K, Maeda K, Ishida-Takagishi M, Ishii G, Ming S, Sun T and Takahashi M. Significance of cancer-associated fibroblasts in the regulation of gene expression in the leading cells of invasive lung cancer. J Cancer Res Clin Oncol 2013; 139: 379-388.

[38] Ivanova S, Polajnar M, Narbona-Perez AJ, Hernandez-Alvarez MI, Frager P, Slobodnyuk K, Plana N, Nebreda AR, Palacin M, Gomis RR, Behrends C and Zorzano A. Regulation of death receptor signaling by the autophagy protein TP53INP2. EMBO J 2019; 38: e99300.

[39] Li HX, Luo X, Liu RX, Yang YJ and Yang GS. Roles of Wnt/beta-catenin signaling in adipogenic differentiation potential of adipose-derived mesenchymal stem cells. Mol Cell Endocrinol 2008; 291: 116-124.

[40] Houschyar KS, Tapking C, Borrelli MR, Popp D, Duscher D, Maan ZN, Chelliah MP, Li J, Harati K, Wallner C, Rein S, Pforringer D, Reumuth G, Grieb G, Mouraret S, Dadras M, Wagner JM, Cha JY, Siemers F, Lehnhardt M and Behr B. Wnt pathway in bone repair and regeneration

- what do we know so far. Front Cell Dev Biol 2018; 6: 170.
[41] Valenta T, Hausmann G and Basler K. The many faces and functions of beta-catenin. EMBO J 2012; 31: 2714-2736.
[42] Enzo MV, Rastrelli M, Rossi CR, Hladnik U and Segat D. The Wnt/beta-catenin pathway in human fibrotic-like diseases and its eligibility as a therapeutic target. Mol Cell Ther 2015; 3: 1.
[43] Sotthibundhu A, Promjuntuek W, Liu M, Shen S and Noisa P. Roles of autophagy in controlling stem cell identity: a perspective of self-renewal and differentiation. Cell Tissue Res 2018; 374: 205-216.
[44] Quan W and Lee MS. Role of autophagy in the control of body metabolism. Endocrinol Metab (Seoul) 2013; 28: 6-11.
[45] Tanida I. Autophagosome formation and molecular mechanism of autophagy. Antioxid Redox Signal 2011; 14: 2201-2214.
[46] You Z, Xu Y, Wan W, Zhou L, Li J, Zhou T, Shi Y and Liu W. TP53INP2 contributes to autophagosome formation by promoting LC3-ATG7 interaction. Autophagy 2019; 15: 1309-1321.
[47] Pankiv S, Clausen TH, Lamark T, Brech A, Bruun JA, Outzen H, Overvatn A, Bjorkoy G and Johansen T. p62/SQSTM1 binds directly to Atg8/LC3 to facilitate degradation of ubiquitinated protein aggregates by autophagy. J Biol Chem 2007; 282: 24131-24145.
[48] Johansen T and Lamark T. Selective autophagy mediated by autophagic adapter proteins. Autophagy 2011; 7: 279-296.
[49] Vidoni C, Ferraresi A, Secomandi E, Vallino L, Gardin C, Zavan B, Mortellaro C and Isidoro C. Autophagy drives osteogenic differentiation of human gingival mesenchymal stem cells. Cell Commun Signal 2019; 17: 98.
[50] Wan Y, Zhuo N, Li Y, Zhao W and Jiang D. Autophagy promotes osteogenic differentiation of human bone marrow mesenchymal stem cell derived from osteoporotic vertebrae. Biochem Biophys Res Commun 2017; 488: 46-52.